

RESEARCH ARTICLE

A satellite-based climatology of fog and low stratus formation and dissipation times in central Europe

Eva Pauli^{1,2}  | Jan Cermak^{1,2}  | Hendrik Andersen^{1,2} ¹Institute of Meteorology and Climate Research, Karlsruhe Institute of Technology (KIT), Karlsruhe, Germany²Institute of Photogrammetry and Remote Sensing, Karlsruhe Institute of Technology (KIT), Karlsruhe, Germany**Correspondence**Eva Pauli, Institute of Meteorology and Climate Research and Institute of Photogrammetry and Remote Sensing, Karlsruhe Institute of Technology (KIT), Karlsruhe, Germany.
Email: eva.pauli@kit.edu**Funding information**

Graduate Funding of German States

Abstract

Knowledge of fog and low stratus (FLS) cloud patterns and life cycles is important for traffic safety, for the production of solar energy and for the analysis of cloud processes in the climate system. While meteorological stations provide information on FLS, a data set describing FLS formation and dissipation times on large spatial and temporal scales does not yet exist. In this study, we use logistic regression to extract FLS formation and dissipation times from a satellite-based 10-year FLS data set covering central Europe. The resulting data set is the first to provide a geographic perspective on FLS formation and dissipation at a continental scale. The patterns found show a clear dependency of FLS formation and dissipation times on topography. In mountainous areas, FLS forms in the night and dissipates in the morning. In river valleys, the typical FLS life cycle shifts to formation after sunrise and dissipation in the afternoon. Seasonal patterns of FLS formation and dissipation show similar FLS formation and dissipation times in winter and autumn, and in spring and summer, with longer events in the former two seasons.

KEYWORDS

Europe, fog, fog dissipation, fog formation, logistic regression, low stratus

1 | INTRODUCTION

Fog and the timing of its formation and dissipation is important for traffic on land, at sea and in the air (Leigh *et al.*, 1998; Pagowski *et al.*, 2004), and is critical for the quality of the prediction of solar power production (Köhler *et al.*, 2017). Fog is also a crucial water source for various ecosystems around the world (Bruijnzeel *et al.*, 2006; Gottlieb *et al.*, 2019) and plays an important role in climate processes (Vautard *et al.*, 2009).

In general, fog can be defined as a cloud touching the ground with a horizontal visibility less than 1 km

(American Meteorological Society, 2012). It can be further classified into different types based on its formation mechanisms. Radiation fog is the most frequent fog type in central Europe (Fuzzi *et al.*, 1992; Gultepe *et al.*, 2007a). It forms through radiative cooling of the ground, a build-up of a temperature inversion and subsequent condensation of the excess water vapour, and is sustained by radiative heat loss at the fog top (Roach, 1995). Geographically, radiation fog occurs more frequently in valleys, such as large river valleys, compared to mountainous areas, as shown by Scherrer and Appenzeller (2014) for the Swiss Plateau and Fuzzi *et al.* (1992) and Bendix (1994) for the

Po Valley mostly in autumn and winter, when the conditions described above are present (Cermak *et al.*, 2009; Egli *et al.*, 2017).

Dissipation of radiation fog can take place through various pathways. After sunrise, the increasing solar radiation leads to a 'burn-off' of fog due to warming of air and mixing of the boundary layer (Roach, 1995; Haeffelin *et al.*, 2010; Maalick *et al.*, 2016). Short-wave radiative warming can also lead to a transition of fog into a low stratus cloud (Maalick *et al.*, 2016). Turbulent heat fluxes can contribute strongly to the loss of liquid water content in the fog layer and thus to fog dissipation (Wærsted *et al.*, 2019). Furthermore, higher wind speeds can lead to the erosion of fog at its top (Bergot, 2016), and high clouds moving over the fog can reduce radiative cooling of the cloud tops, resulting in the dissipation of the fog layer (Roach, 1995). Land surface characteristics can also modulate fog patterns, for example, over cities that often feature 'fog holes' over urban areas (Yan *et al.*, 2020).

The knowledge of formation and dissipation time of fog relies strongly on ground-based observational data and localized process studies with numerical models such as large-eddy simulations. These have been conducted for example in France (e.g., Haeffelin *et al.*, 2010; Dupont *et al.*, 2012; Wærsted *et al.*, 2019; Karimi, 2020) or in the Netherlands (Duykerke, 1991; Steeneveld and de Bode, 2018) over time-scales ranging from 6 days (Dupont *et al.*, 2012) up to 7 years (Wærsted *et al.*, 2019). According to these studies, radiation fog usually forms during the night through nocturnal cooling (Roach, 1995) and dissipates a few hours after sunrise (Haeffelin *et al.*, 2010; Bergot, 2016; Steeneveld and de Bode, 2018). While these studies provide insights on the small-scale processes of fog formation and dissipation, large-scale processes play a major role as well. Thus, data at large spatial scales are necessary to obtain knowledge on fog formation and dissipation processes across different landscapes.

Geostationary satellite data have proven suitable for the observation of fog over large spatial scales, for example, over Europe (Cermak *et al.*, 2009; Cermak and Bendix, 2011; Egli *et al.*, 2017), North America (Ellrod and Gultepe, 2007; Gultepe *et al.*, 2007b; Torregrosa *et al.*, 2016) and the Namib desert (Andersen and Cermak, 2018). They provide information about fog and low stratus clouds over a large spatial area and with a high temporal resolution. When no ground information is available, fog and low stratus (FLS) are typically treated as a single category (Cermak and Bendix, 2011). Based on Cermak and Bendix (2007; 2008) a FLS dataset has been created by Egli *et al.* (2017) which provides information about FLS cover over Europe for each 15-min interval over 10 years. This dataset has been used previously for the study of large-scale drivers of FLS using machine learning (Pauli *et al.*, 2020). Still, it has

to be considered that not all FLS situations can be detected accurately by geostationary satellite data, as small-scale FLS features, classification errors and multi-layer cloud situations can lead to misclassifications (Cermak and Bendix, 2008; Cermak, 2018).

The goal of this study is to analyse and discuss the spatial patterns of continental FLS formation and dissipation times over central Europe. Both formation and dissipation times are extracted from an existing, well-validated satellite-based binary FLS data set by Egli *et al.* (2017) with a logistic regression. The seasonal differences of the extracted formation and dissipation times are analysed across Europe and the regional applicability and detail are shown in a regional study in southern Germany. The resulting novel data set gives information on FLS formation and dissipation times over continental Europe and over 10 years, on spatial and temporal scales not previously investigated. The guiding hypothesis of this study is as follows. The timing of fog and low stratus formation and dissipation in central Europe is mainly dependent on topography. Its specific patterns are further impacted by the distance to the coast and local- to regional-scale modulations of the relevant meteorological drivers of FLS (Pauli *et al.*, 2020).

2 | DATA & METHODS

2.1 | Data

The basis of this study is an FLS data set by Egli *et al.* (2017) which covers Central Europe over the years 2006–2015. The FLS data set is created using data from the Meteosat Spinning Enhanced Visible and Infrared Imager (SEVIRI) and a number of threshold tests that are based on the Satellite-based Operational Fog Observation Scheme (SOFOS) by Cermak (2006). FLS in the Egli *et al.* (2017) data set is defined as a low stratiform cloud with liquid droplets not exceeding a size of 20 μm (Egli *et al.*, 2017) but radiation fog and other stratiform clouds are not distinguished.

The FLS data set contains binary information, that is, 1 if FLS is present and 0 if FLS is not present. The data set is available for every 15 min time slot of SEVIRI at its native resolution (3 \times 3 km at nadir). At twilight, no FLS detection is possible, leading to ϵ FLS not present ϵ (0) values in the original data set during about four to five 15-min time steps during each twilight episode. After exploring different treatments of those twilight values (keeping them at 0, setting them to NAN (not a number), temporal interpolation), setting them to NAN has been chosen as the most suitable method in this study, as this avoids the introduction of false information. However, on the basis of the Egli

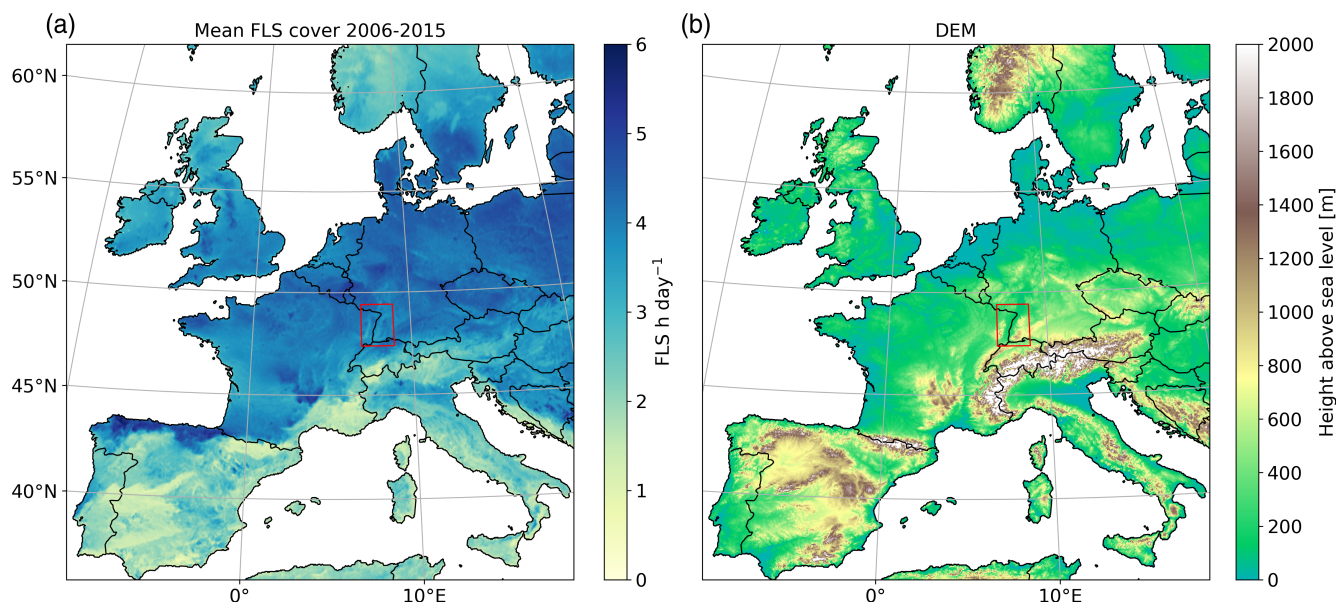


FIGURE 1 (a) Mean fog and low stratus cover in Central Europe from 2006 to 2015 (data set by Egli *et al.* (2017)) and (b) mean height above sea level. The Upper Rhine Valley, used as a regional study area for the demonstration of the algorithm and to show the spatial detail of the results, is indicated by the rectangle [Colour figure can be viewed at wileyonlinelibrary.com]

et al. (2017) data set, we are unaware of formation and dissipation time at twilight.

To provide an overview of the data used for the identification of FLS formation and dissipation time, we show the mean FLS cover in Figure 1a. The mean FLS cover over the study domain of Central Europe generally shows higher FLS frequencies over the northern latitudes and in large-scale river valleys (Figure 1a). In mountain ranges as well as in the Mediterranean, FLS frequencies are low. The dependency of FLS cover on topography can also be seen by looking at both mean FLS cover (Figure 1a) and mean height above sea level over the study area (Figure 1b). The data set can be used in various research applications, such as the investigation of large-scale drivers of FLS (Pauli *et al.*, 2020).

2.1.1 | Validation of FLS data used

In the work presented here, we use the existing and thoroughly validated FLS data set by Egli *et al.* (2017) to extract FLS formation and dissipation times by applying logistic regression. While we do create a novel FLS formation and dissipation times data set, the technique we use is not an FLS detection technique but a statistical interpretation of an already existing, thoroughly validated, satellite-based FLS data set. In this section, we provide an overview of the validation results of studies using the SOFOS algorithm for the detection of fog and low clouds (Cermak, 2006; Cermak and Bendix, 2007; 2008; Egli *et al.*, 2017). Details

on the validation procedures can be found in the relevant publications.

For the validation of the SOFOS algorithm, Meteorological Aviation Routine Weather Reports (METARs) were used, as these are available with a high temporal frequency (at least every hour) and well distributed over continental Central Europe. In general the SOFOS algorithm detects FLS very accurately (Cermak, 2006; Cermak and Bendix, 2007; 2008; Egli *et al.*, 2017). Cermak (2006) and Cermak and Bendix (2008) found that 70 to 85% of FLS situations are detected by the scheme. Situations where FLS is not detected can to a large degree be explained by overlying clouds, which are present above FLS about 25% of the time in the study domain (Cermak, 2018). False alarms are rare, that is, a pixel classified as FLS is almost never either clear or covered by a different cloud type (Cermak and Bendix, 2008). Similar to the other studies using the SOFOS algorithm, about 80–90% of FLS and no-FLS situations are classified correctly in the Egli *et al.* (2017) data set used for the extraction of FLS formation and dissipation time. The geographic patterns of validation scores show higher validation scores in continental areas with radiative FLS events as opposed to coastal areas, where advective FLS events prevail (Egli *et al.*, 2017).

We acknowledge the constraints that a satellite-based FLS climatology has when compared to ground observations. Nevertheless the good validation results show that this FLS data set can be used to derive an FLS formation and dissipation climatology as shown in the study at hand.

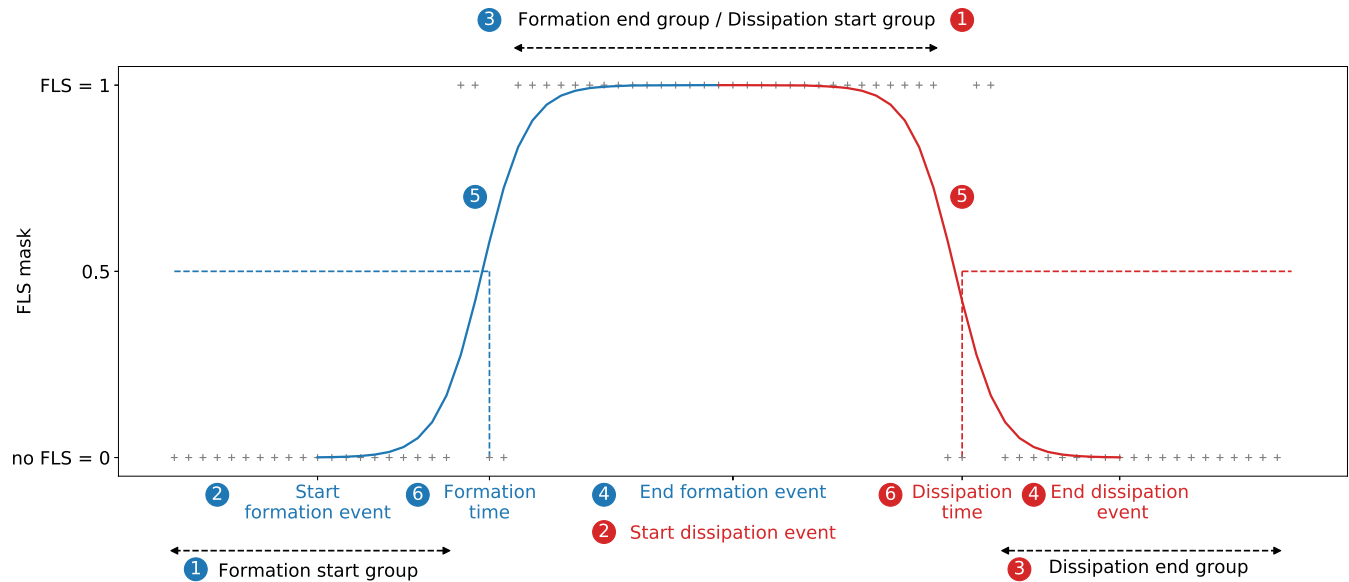


FIGURE 2 Workflow for the identification of FLS formation and dissipation times with logistic regression using an artificial example. Steps for the identification of formation time are plotted in blue, and the corresponding steps for the identification of dissipation time are plotted in red. Black crosses mark the binary FLS values [Colour figure can be viewed at [wileyonlinelibrary.com](https://onlinelibrary.wiley.com/doi/10.1002/qj.4272)]

2.2 | Methods

In this study, we apply logistic regression to statistically interpret the binary FLS data set by Egli *et al.* (2017) to determine FLS formation and dissipation times. After the algorithm is completed, a novel FLS formation and dissipation data set exists, which is derived from the original binary FLS data set by Egli *et al.* (2017). We then analyse this new data set of formation and dissipation time in the results section. In the following, we give a general overview on logistic regression and then describe the algorithm which applies logistic regression to the binary FLS time series described above.

Logistic regression is used for binary or categorical data and in this study predicts the probability of a data point belonging to one of the binary classes (Lever *et al.*, 2016; Bisong, 2019). Mathematically, the probability can be expressed as:

$$p(t) = \frac{1}{1 + \exp(-b_0 - b_t * t)}, \quad (1)$$

where p is the probability, t the time, b_0 the intercept and b_t the slope. While multiple predictor variables can be used in logistic regression, in this study, time is the only predictor. The transition from one state to another and its associated predictor value is called the “decision boundary” (Bisong, 2019). Here, this decision boundary is used to determine the time of FLS formation and dissipation.

In the atmospheric sciences, logistic regression has previously been used for the detection of hail (López and

Sánchez, 2009) or to forecast the probability of extreme precipitation events (Applequist *et al.*, 2002; Herman and Schumacher, 2018). It has also been applied to predict the occurrence of orographic cloud cover (Wu and Zhang, 2013) or to forecast the probabilities of low visibility conditions at an airport site (Kneringer *et al.*, 2019).

2.2.1 | Algorithm

In the following we describe the algorithm which identifies FLS formation and dissipation time based on the binary cloud mask. The algorithm consists of six steps. These steps are similar for formation and dissipation time but are conducted separately. The algorithm is applied to each valid FLS event (defined below) and to each pixel over the years 2006–2015. The steps described below are marked with the corresponding numbers in Figure 2.

To apply the logistic regression to the data set, at first an FLS formation/dissipation event has to be identified (step 1). In the case of FLS formation, this means that over a period of at least ten consecutive 15-min time steps (2.5 hr) no FLS has to be present (cloud mask = 0). In the case of FLS dissipation, the requirement is similar (FLS present (cloud mask = 1) for ten consecutive 15-min time steps). By choosing a minimum value of 2.5 hr we are likely to exclude random misclassifications in the original FLS data set as well as advective FLS events with fast changes between FLS and no-FLS. One should note that the results can thus only be interpreted with respect

to such longer-lasting FLS events, and may not be representative of FLS events with a shorter life cycle. After identification of such a start group, its temporal centre point is then used as the start of the FLS formation or dissipation event (step 2). Looking at the artificial example in Figure 2, the start group of the formation event (blue curve) has 20 consecutive 15-min time steps of no-FLS. The starting point is then defined as the centre, in this case at the tenth time step of no-FLS.

The end group of a given FLS formation or dissipation event is defined similarly to the start group. In the case of FLS formation, this means that for ten consecutive 15-min time steps FLS has to be present (cloud mask = 1), and in case of dissipation FLS has to be absent for ten consecutive 15-min time steps (step 3). The end group has to be present within 30 hr from the start of the formation or dissipation event. By choosing a time period of 30 hr, it is possible to capture FLS events that persist for longer than a day. If no end group can be identified within 30 hr of the start of the formation/dissipation event (step 2), the formation/dissipation event is omitted, and no time is determined by the algorithm.

Similar to the determination of the start of the formation/dissipation event, the end of such an event is then set to be the centre of the corresponding end group (step 4). In the artificial example in Figure 2, the end group of the formation event contains 30 15-min time steps with FLS, with the end point of formation defined in the centre of the group at time step 15. During twilight, the groups of consecutive FLS or no-FLS are interrupted by NAN values as outlined in Section 2.1. If the remaining groups then do not fulfill the requirement of ten consecutive FLS or no-FLS values, this leads to a potential loss of start and end groups.

Following the identification of the start and end points of the FLS formation/dissipation events, logistic regression is applied to the binary time series between the start and end points to model the probability of FLS presence (step 5). Then, the decision boundary is used to depict the formation and dissipation times (step 6). For formation, the first 15-min time period in which the probability modelled by the logistic regression exceeds 0.5 is defined as the formation time. For dissipation, the first 15-min time period where the probability falls below 0.5 is defined as the dissipation time.

After the calculation of the formation/dissipation time, these six steps are repeated for each identified start group for each pixel separately. While the formation and dissipation situation displayed in Figure 2 can be considered as an ideal example, with a dissipation event following a formation event right away, there is also the possibility that a dissipation event is not identified right after a formation event. This occurs when an end of the dissipation event cannot be identified within 30 hr, due to alternating FLS

and no-FLS values. If the requirements discussed above are not fulfilled by either a potential formation or dissipation event, it is possible that multiple FLS formation or dissipation events are identified one after another. This leads to slight differences in the number of formation and dissipation events identified by the algorithm, which is discussed in Section 3.1.

2.2.2 | Discussion of algorithm uncertainties

It is clear that the quality of the derived FLS formation and dissipation time products is dependent on the quality of the underlying FLS data set. Therefore, systematic and random errors in the FLS data set will propagate to our classification. However, by focusing on temporally persistent FLS events, we reduce effects of random misclassifications in the data set. Another uncertainty of the derived FLS formation and dissipation time products is introduced by differences in the characteristics of the binary variability of each specific FLS event (Figure 3). An abrupt, temporally coherent change between the binary classes (little alternation between FLS and no-FLS values), leads to a higher absolute value of the slope and a steep curve fit. This leads to either the classic sigmoid shape (Figure 3a, d) or a very steep transition (Figure 3b, e), both of which are easy to interpret with respect to FLS formation and dissipation time. However, in the case of frequent changes between FLS and no-FLS values of an FLS event considered, the fitted logistic curve is flat and the slope value approaches zero (Figure 3c, f). These flat curves are difficult to interpret with respect to an FLS formation/dissipation time, and are thus excluded from the data set. We define these valid situations to feature a slope of $> |0.1|$. This threshold was defined by conducting a thorough visual analysis of different events and their corresponding curve shapes. The exclusion of these high-uncertainty events leads to an average reduction of 9% of FLS events per pixel.

2.3 | Case illustration: 7 February 2011

To illustrate how formation and dissipation time are derived from the binary FLS masks, a dissipation case from 7 February 2011 over the Upper Rhine Valley in Germany is presented in the following. The mean FLS cover and topography of the region are shown in Figure 4.

Radiation fog is a frequent phenomenon in the Upper Rhine Valley, especially in the colder months (Kalthoff *et al.*, 1998; Bendix, 2002; Bendix *et al.*, 2006; Egli *et al.*, 2017). In this rift valley between the Vosges mountains to the west and the Black Forest mountains to the east (visible in Figure 4b and roughly depicted in Figure 4 with the

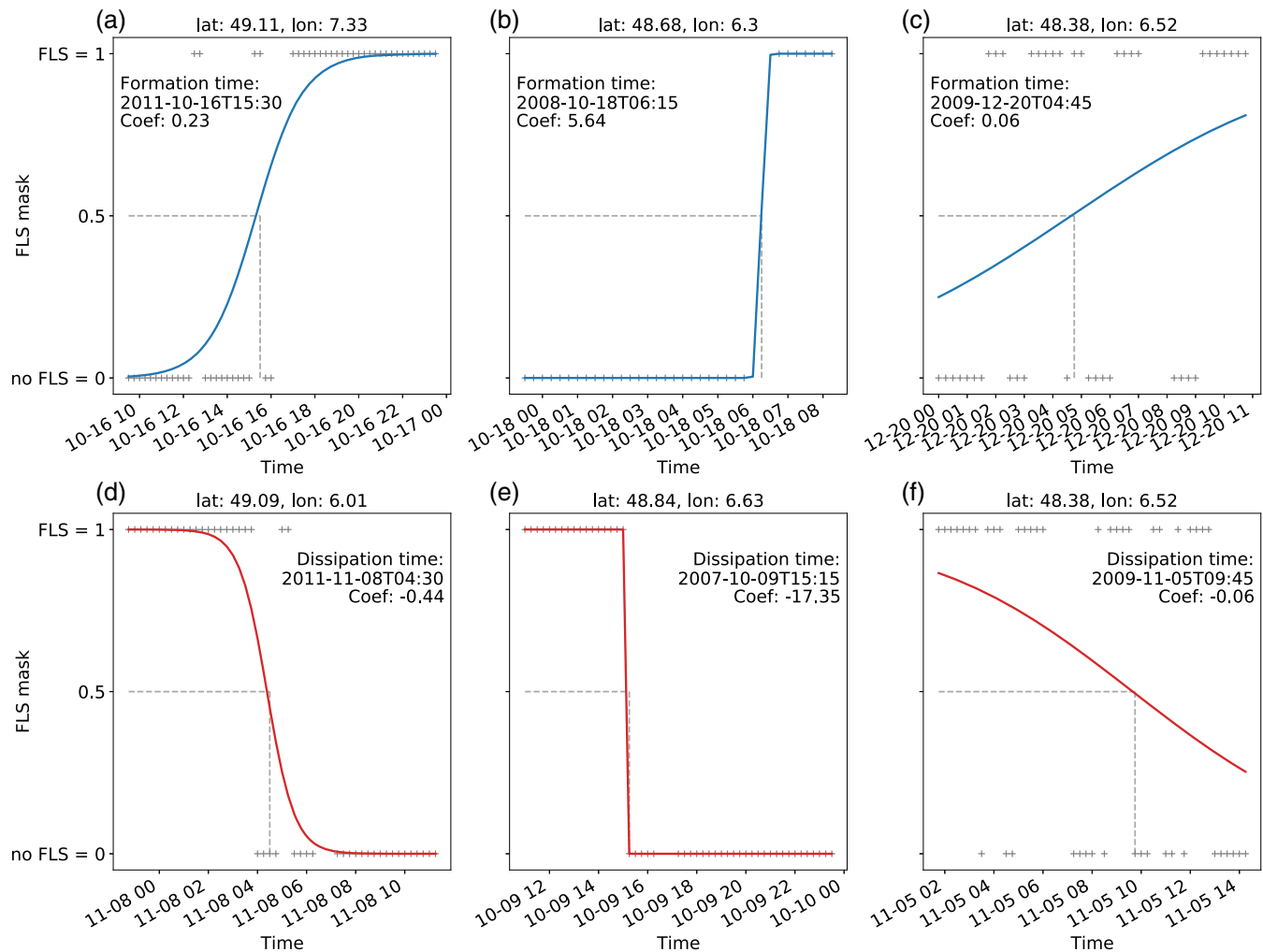


FIGURE 3 Logistic regression curves for three formation situations (a–c) and three dissipation situations (d–f). The situations in (a, d) have a classic sigmoid shape and the situations in (b, e) have a sharp transition. The curves in (c, f) do not fulfill the slope requirements (coefficient $> |0.1|$). The Coef parameter denotes the slope of the logistic regression curve [Colour figure can be viewed at wileyonlinelibrary.com]

500 m contour), FLS occurs more frequently in the valley than on the mountain ridges (Figure 4a).

The case illustration of 7 February 2011 focuses on three pixels in the Upper Rhine Valley (at locations A, B, C), all of them located in France. As can be seen in the binary FLS maps (Figure 5), FLS is present mainly in the northern part of the valley on the morning of 7 February and then dissipates during the day. To illustrate the derivation of the dissipation time, the binary time series at the three locations is extracted (Figure 6). A logistic regression is calculated for all time series and the time stamp where the probability of the binary value being equal to 1 falls below 0.5 is assigned to be the dissipation time. In line with the binary FLS masks in Figure 5, FLS at location B dissipates first (0930 UTC) followed by location A (dissipation at 1145 UTC). FLS at location C is most stable and dissipates in the afternoon (1430 UTC).

The approach presented here for the identification of dissipation time at the three locations is then applied to each pixel of the study area, for each identified FLS formation and dissipation event.

3 | RESULTS

3.1 | Number and duration of FLS events

As a first view of the data set, the number of formation events for which a formation time was calculated is shown (Figure 7a). The number of formation events is representative of the number of dissipation events, which is very similar with a difference around ± 10 events per pixel. As discussed above, this slight difference is present since not every formation event is followed by a dissipation

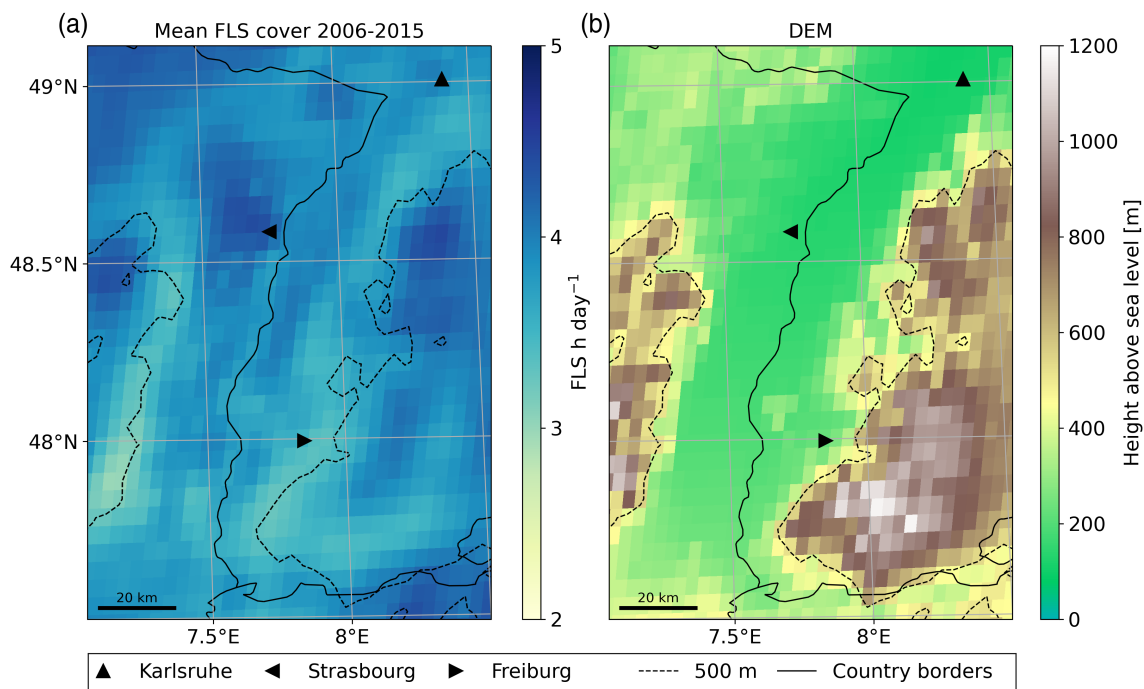


FIGURE 4 (a) Mean fog and low stratus cover in the Upper Rhine Valley from 2006 to 2015 (data set by Egli *et al.* (2017)) and (b) mean height above sea level. The country border between France and Germany also marks the course of the river Rhine. The black dashed line depicts 500 m height above mean sea level [Colour figure can be viewed at wileyonlinelibrary.com]

event which fulfills the requirements discussed above, and *vice versa*. The geographic patterns of the number of detected formation events are similar to the geographic patterns of mean FLS cover (Figure 1). A high number of formation events is identified in the northeast of the study area (1,000–1,200 events over 10 years), as well as in the Po Valley and at the north coast of Spain. Moreover, a higher number of formation events is detected over cities, especially visible over Milan and Paris. This is likely a systematic error of the FLS data set used, as higher FLS cover over cities can also be seen in Figure 1a. The overestimation of FLS cover over cities is likely due to their high reflectance in the $3.9 \mu\text{m}$ channel due to solar contamination during daytime, which is likely to lead to a false identification of clouds during this time (EUMETSAT, 2019). Higher daytime FLS cover over urban pixels compared to the rural surroundings can be observed in the mean diurnal course of FLS cover over London, Paris and Milan (Figure S1).

A low number of formation events (300–400 events over 10 years) is detected over the Mediterranean and over mountain ranges (Alps, Pyrenees). The same geographic patterns described here for the number of formation events apply to the number of dissipation events.

The FLS duration is calculated as the difference between dissipation time and formation time for one FLS event for each pixel. To decrease the influence of

outliers, the median instead of the mean is shown here. The geographic patterns of duration are similar to the FLS mean map and the number of dissipation events. FLS events tend to be longer in the northeastern part of the study area (400–600 min) and shorter in the Mediterranean (200–300 min). The geographic patterns of median duration are also similar to those of the mean FLS cover and the number of formation events. This is also visible when normalizing the three quantities (Figure S2) to enhance comparability. Still, the spread of values is lower for the median duration than the mean FLS cover and the number of formation events.

3.2 | Most frequent formation and dissipation times

For further analysis, the timestamps of formation and dissipation times are converted into % values as a function of day length (sunrise–sunset) for formation or dissipation during the day or as a function of night length (sunset–sunrise) for nighttime formation and dissipation. This is done to make formation and dissipation time comparable across seasons and latitudes.

To facilitate interpretation, these % values are then assigned to different classes of day- or nighttime (Table 1). To produce climatological maps of the most frequent

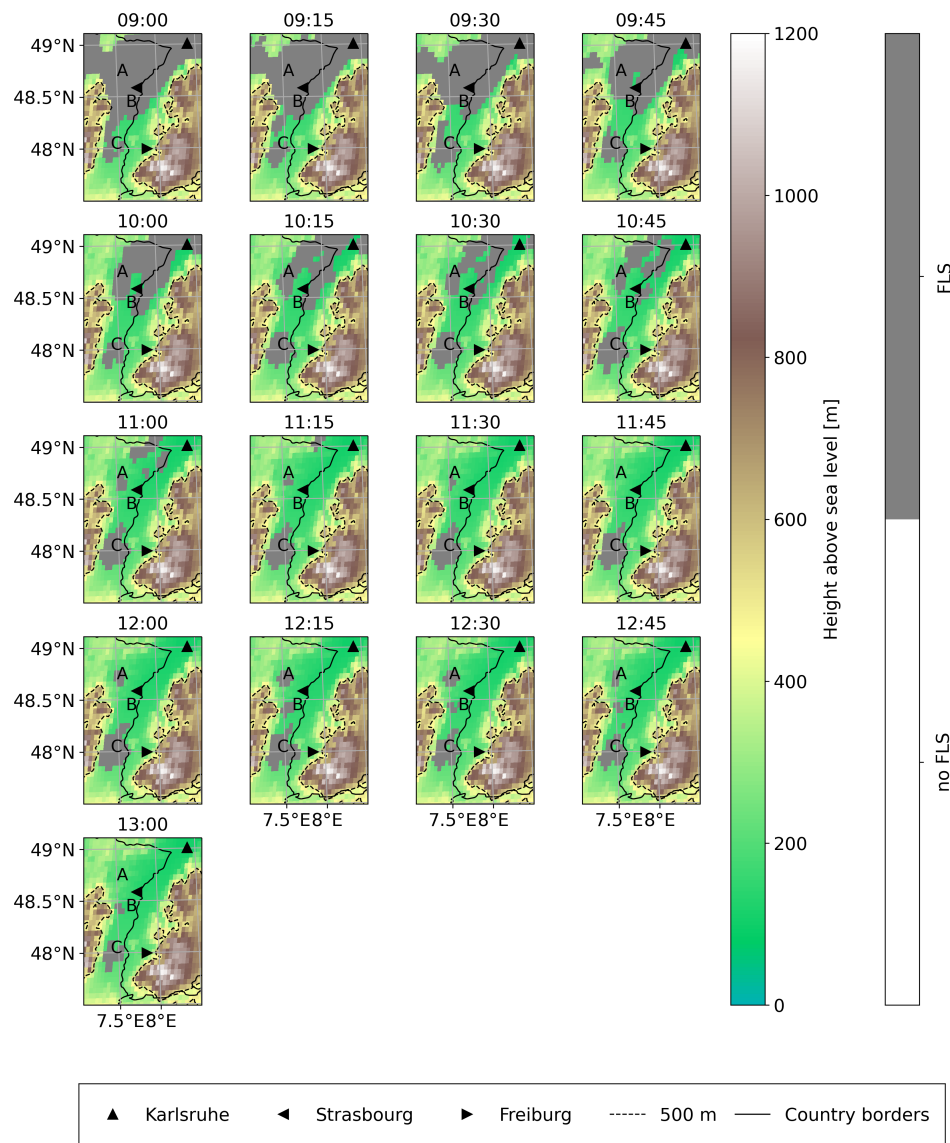


FIGURE 5 Binary 15-min FLS masks (data set by Egli *et al.* (2017)) from 0900 to 1300 UTC on 7 February 2011. Pixels with FLS cover are grey, pixels without FLS are transparent. The background is a topographic map of the region. The country border between France and Germany also marks the course of the river Rhine. The black dashed line depicts 500 m height above mean sea level [Colour figure can be viewed at wileyonlinelibrary.com]

formation and dissipation time, the mode of these classes is used for each pixel over the entire time period (Figure 8) and depending on the season (Figure 9).

When considering the entire study period (Figure 8), FLS forms most frequently around midnight in large parts of the study area such as areas of France, Germany and Italy, where secondary mountain ranges as well as rather flat areas, such as the Danube valley, are present. In the high-altitude mountain ranges (Alps, Pyrenees) and on the north coast of Spain, formation is most frequently around sunset. In the inner plateau of central Spain, western France and in the Po Valley, FLS forms most frequently around sunrise and in the morning.

The geographic distribution of most frequent dissipation time shows similar spatial patterns of equal dissipation time as was seen for formation time. On the north coast of Spain, and in high-altitude mountains such as the Pyrenees and the Alps, FLS dissipates most frequently

around sunrise or in the morning. In secondary mountain ranges such as the Massif Central in southern France and the pre-alpine areas of southern Germany, dissipation occurs mainly in the morning or around midday. In the low-altitude areas of central Europe, such as northern France, northern Germany and Poland but also in the inner plateau of Central Spain, dissipation occurs most frequently in the afternoon.

The seasonal patterns of formation and dissipation times tend to be similar in winter (DJF) and autumn (SON) and in spring (MAM) and summer (JJA) (Figure 9). In winter and autumn, FLS formation occurs most frequently in the evening or during the night and dissipation around midday or in the afternoon. In spring and summer FLS typically forms later, most frequently around sunrise, but does not last as long as during winter and dissipates in the morning. The detailed geographic patterns for each season are described below.

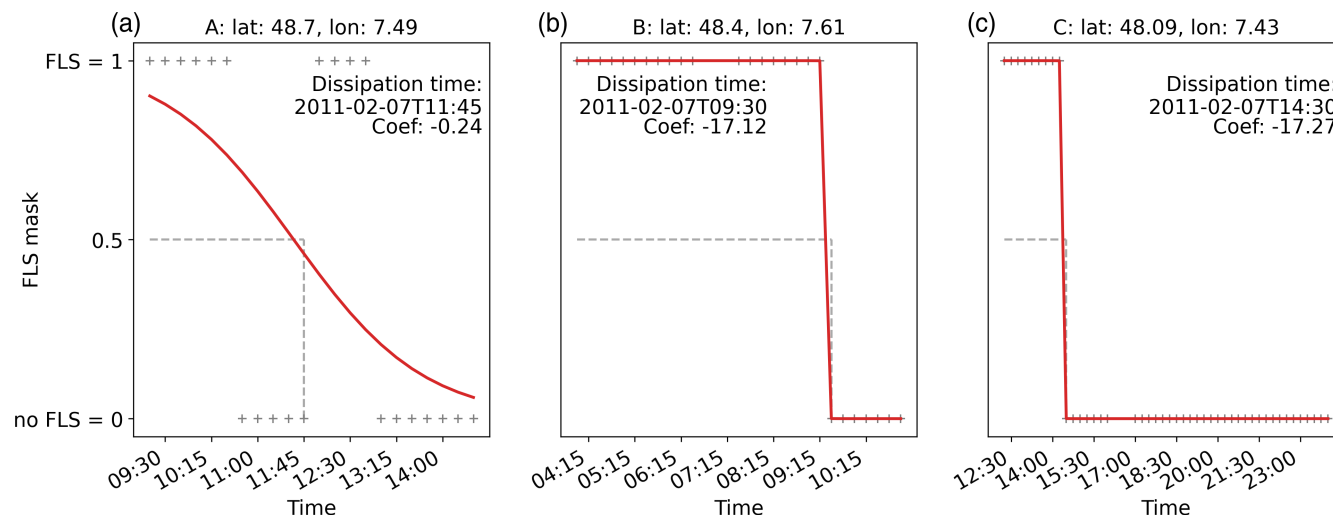


FIGURE 6 Logistic regression curves for the dissipation events on 7 February 2011 at the three locations A, B, C marked in Figure 5. The Coef parameter denotes the slope of the logistic regression curve [Colour figure can be viewed at wileyonlinelibrary.com]

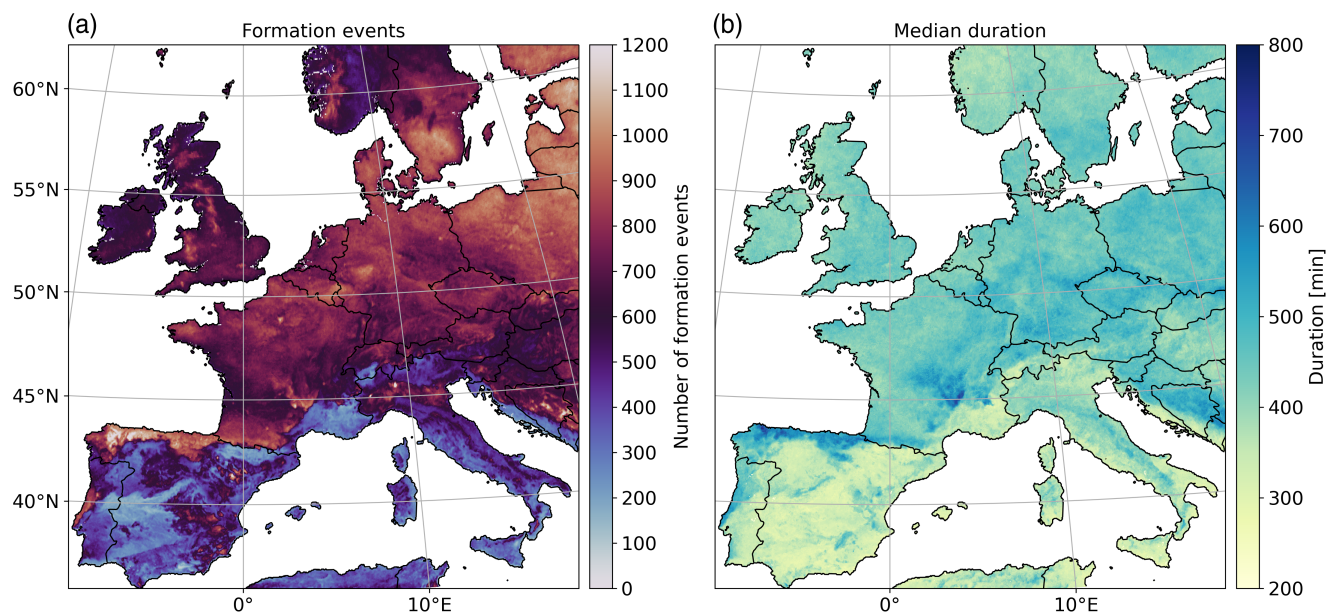


FIGURE 7 (a) Number of formation events identified by the algorithm, and (b) the median of the duration of all FLS events in which both formation and dissipation times could be determined. Both are calculated over the entire period (2006–2015) [Colour figure can be viewed at wileyonlinelibrary.com]

In winter FLS forms most frequently in the evening or around midnight, except for large areas in western France and the inner plateau of central Spain, where formation most frequently takes place in the morning. During this time, FLS dissipates most frequently in the afternoon in most regions, and earlier (in the morning or around midday) in parts of the Alps, in the secondary mountain ranges of southern Germany or southern Italy.

In spring the most frequent formation time shifts to sunrise or to the morning hours in large parts of France, central Spain and in the Po Valley. On the north coast of

Spain, southern France, in the Pyrenees and in the Alps, FLS forms most frequently at sunset. Dissipation most often takes place in the morning or around midday in most parts of the study area. In the Po Valley and in large parts of Poland, FLS is more persistent and most frequently dissipates in the afternoon.

In summer FLS formation patterns are spatially diverse, with formation at sunset (central Germany), around sunrise (Po Valley) or in the morning (France). This could be influenced by the lower number of formation events in summer compared to other seasons in most

TABLE 1 Day- and nighttime classes with respective % ranges

Daytime			Nighttime		
Class number	Class name	% Range	Class number	Class name	% Range
1	Sunrise	0–12.4	1	Sunrise	87.5–100
2	Morning	12.5–37.4	8	Night	62.5–87.4
3	Midday	37.5–62.4	7	Midnight	37.5–62.4
4	Afternoon	62.5–87.4	6	Evening	12.5–37.4
5	Sunset	87.5–100	5	Sunset	0–12.4

parts of the study area (compare Figure S3). A clear pattern of formation at sunrise is visible at the coast of the Mediterranean Sea. Dissipation in summer is most frequently in the morning in large parts of the central study area. FLS dissipates earlier (around sunrise) at the northern coast of Spain and in the Alps, and later (in the afternoon) in western France. Still, these patterns should be interpreted with care, as FLS occurrence is low in most of the Mediterranean in spring and summer (compare hatched areas of Figure 9).

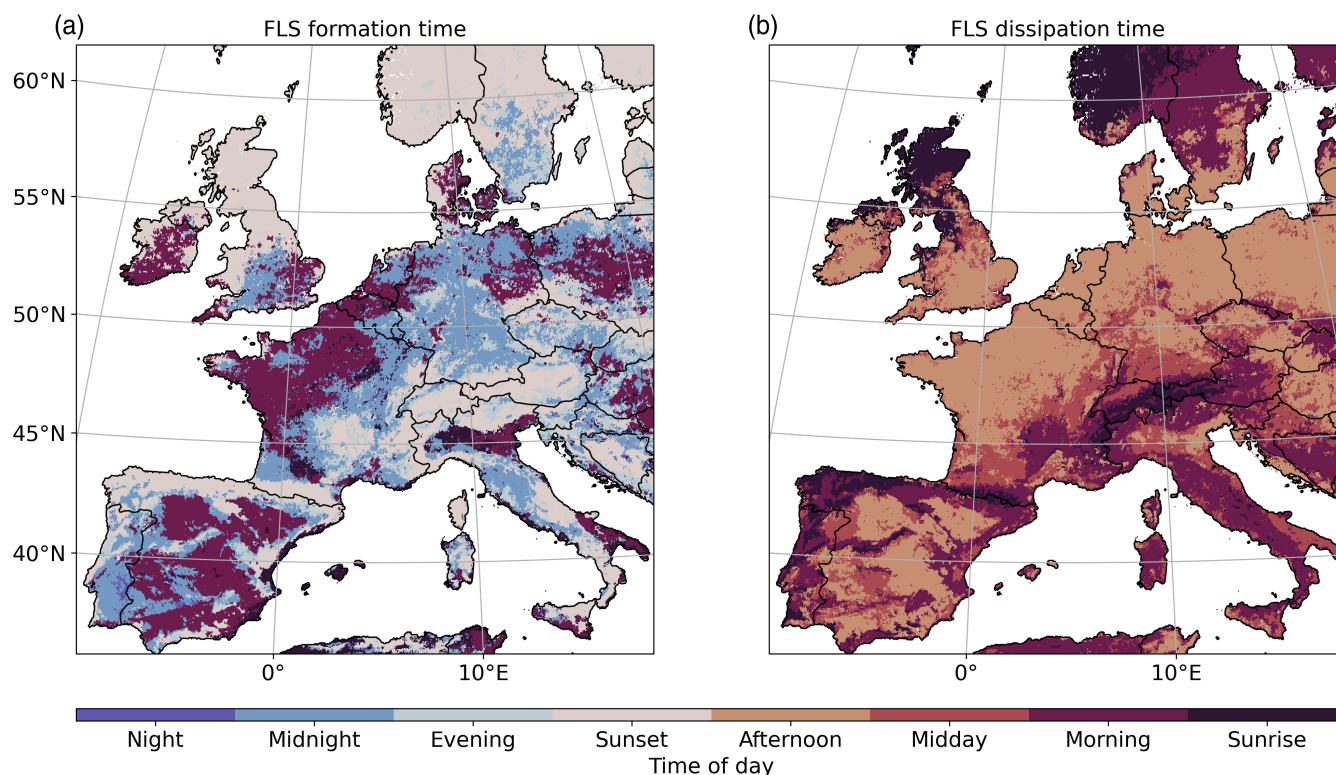
In autumn FLS formation shifts again towards nighttime hours in most of the study area, except for parts of France and Spain, where FLS forms most frequently

in the morning. FLS dissipation also shifts to afternoon hours in most parts of the study area. In the Alps and the Pyrenees, FLS most frequently dissipates at sunrise, in southern Germany around midday.

3.3 | Regional study: Upper Rhine Valley, Germany

While the formation and dissipation times data set can be used to produce climatological maps for Europe, it can also be used for a more thorough investigation of formation and dissipation patterns in regional studies. Such a regional study is presented here by looking closely at formation and dissipation patterns in the Upper Rhine Valley (red rectangle in Figure 1 and introduced in Section 2.3) in southern Germany. The FLS patterns present in that region are likely to be influenced by local to regional modulations of the synoptic-scale weather patterns. Thus the Upper Rhine Valley is an ideal region to showcase the level of spatial detail provided by the novel data set.

The most frequent formation and dissipation time over the complete period (Figure 10a) shows two distinct patches of formation and dissipation anomalies (at $\sim 7.5^\circ\text{E}$, 48°N , and at around 48.7°N). At these locations, formation is observed to be in the morning and dissipation in the

**FIGURE 8** Most frequent (a) formation and (b) dissipation times over the entire study period (2006–2015) [Colour figure can be viewed at [wileyonlinelibrary.com](https://onlinelibrary.wiley.com/doi/10.1002/qj.4272)]

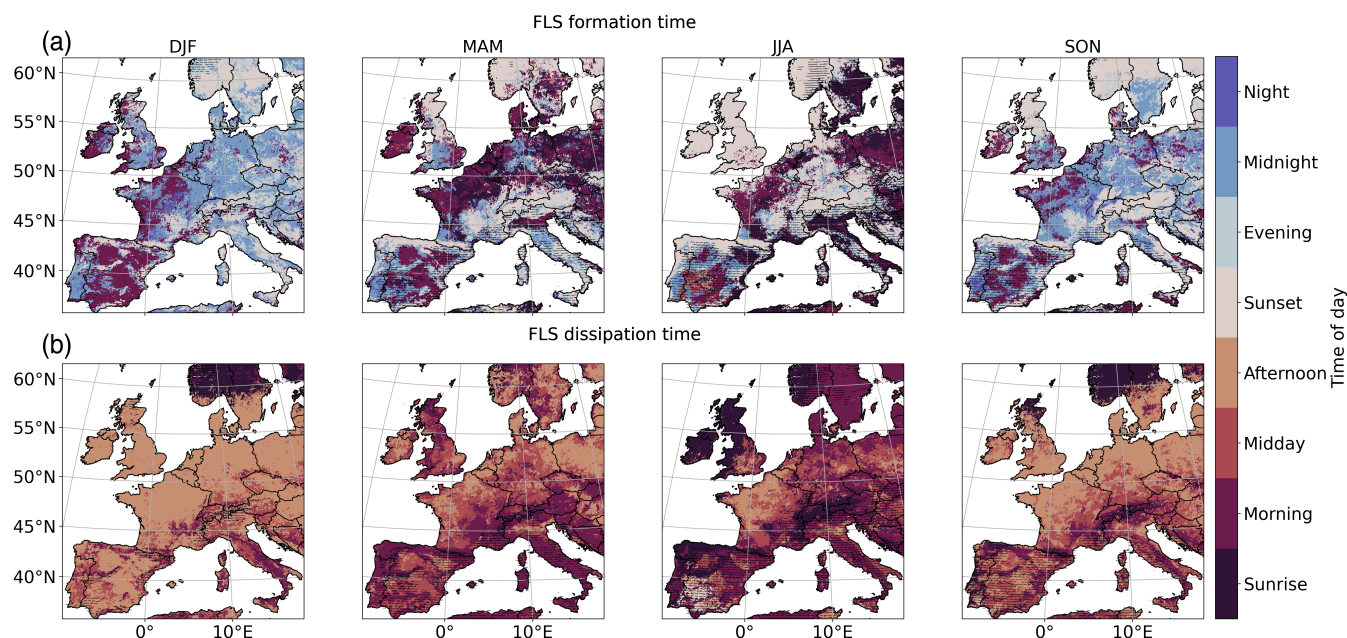


FIGURE 9 Most frequent (a) formation and (b) dissipation times for DJF, MAM, JJA and SON from 2006 to 2015. Pixels with a mean seasonal FLS occurrence of less than 2 hr-day^{-1} are marked with a horizontal line [Colour figure can be viewed at [wileyonlinelibrary.com](https://onlinelibrary.wiley.com/doi/10.1002/qj.4272)]

afternoon (Figure 10a, e). Thus FLS formation and dissipation at these patches are much later than in other places of the Upper Rhine Valley, where FLS usually forms around sunset or around midnight and dissipates in the morning or around midday. While the anomalies are clearly visible in the annual averages, they are especially pronounced in MAM, with formation in the morning and dissipation in the afternoon extending over the eastern slopes of the Vosges (Figure 10b, f).

The percentage of values that fall into the most frequent formation and dissipation time classes relative to all formation and dissipation situations provides a measure of the representativeness of the mode as a proxy for the typical formation and dissipation time for each pixel (Figure 10c, d, g, h). The percentage of values in the most frequent class lies around 15–20% for the formation over the complete year and rises to values around 20–25% in MAM and is highest in the anomalous patches described above. Considering the dissipation, the geographic distribution of % values is similar but on average 10% higher than formation, showing that the temporal variability in dissipation time is lower than the formation time.

This case-study provides two important insights into the novel formation and dissipation data set. First of all, the relatively high spatial and temporal resolution (native SEVIRI resolution; Section 2.1) make it a useful product to study regional formation and dissipation patterns. Secondly, the dissipation time features a lower temporal variability than the formation time, as evidenced by

the systematically higher fraction of events in the most frequent class. Over most of the study area, more than two thirds of dissipation events occur during the day, whereas formation time is equally distributed between daytime and nighttime in large parts of the study area (Figure S4). This is likely due to a higher number of possible formation pathways and thus formation times, whereas dissipation is strongly influenced by solar radiation. We evaluate this further in the discussion below.

4 | DISCUSSION

The geographic patterns of formation and dissipation time clearly underline the role of topography for the occurrence and development of FLS events. In large mountain ranges such as the Alps or the Pyrenees, FLS forms earlier (around sunset) than in lower terrain but also dissipates earlier (around sunrise). These geographic patterns may be interpreted as the signature of regionally characteristic processes influencing FLS formation and dissipation. It is likely that formation at sunset in those mountain ranges is due to advected FLS layers, especially on the windward slopes of those ranges, for example on the northern slopes of the Pyrenees. After sunrise, these FLS layers are likely to be ‘burned-off’ as the sun reaches the mountain tops first. In the Po Valley in Italy or in the inner plateau of Central Spain, FLS formation is likely to be due to nocturnal cooling and a subsequent transition into a low stratus cloud

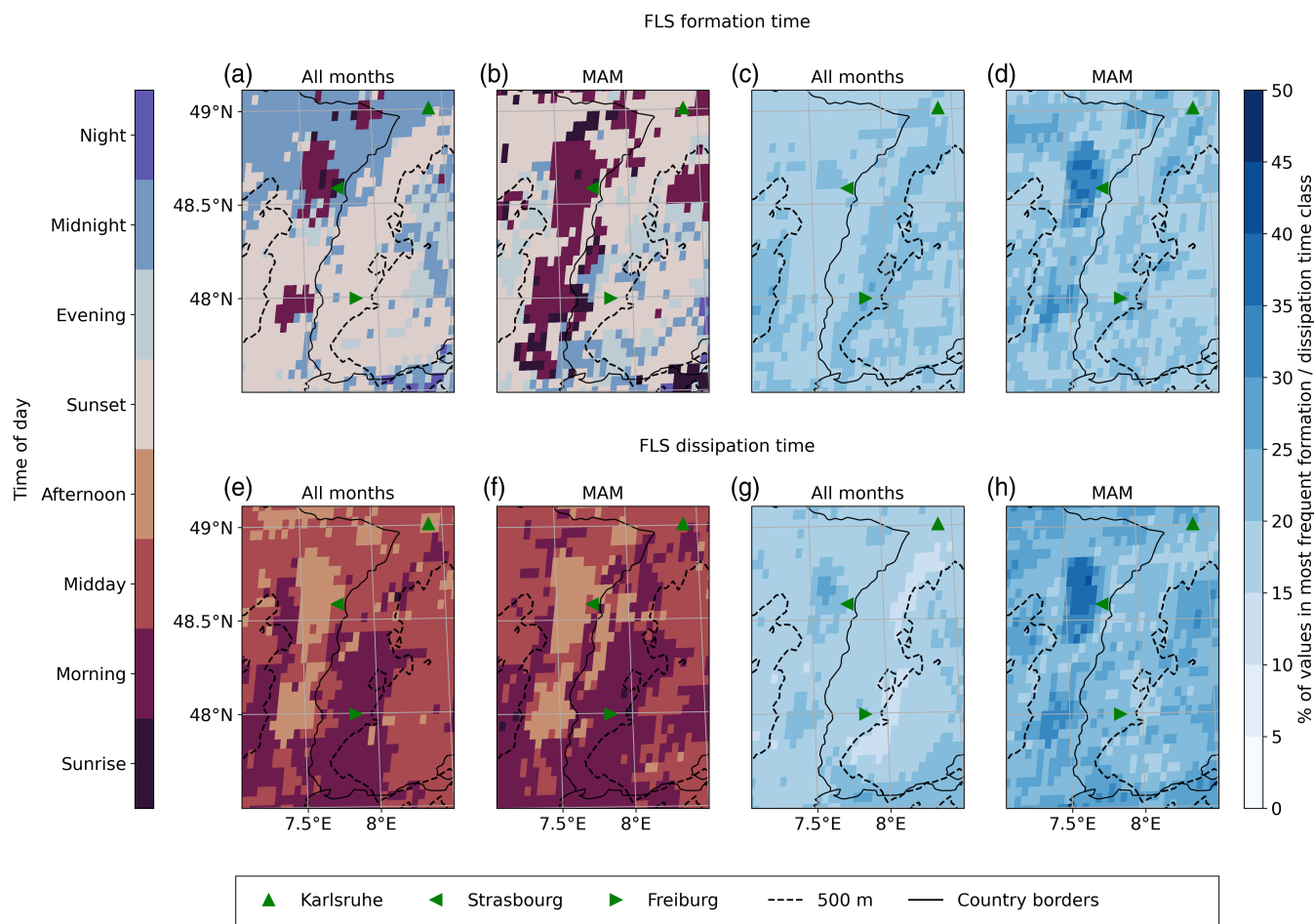


FIGURE 10 Most frequent (a, b) formation and (e, f) dissipation times in the Upper Rhine Valley and the corresponding % of values contained in the most frequent (c, d) formation and (g, h) dissipation class for the complete time period (all months) and in spring (MAM). The country border between France and Germany also marks the course of the river Rhine. The black dashed line depicts 500 m height above mean sea level [Colour figure can be viewed at [wileyonlinelibrary.com](https://onlinelibrary.wiley.com/doi/10.1002/qj.4272)]

(Roach, 1995). Other potential processes involved could be topography-induced drainage flows and turbulence (Price, 2019).

In smaller mountain ranges (e.g., the Black Forest), the dependence of formation and dissipation time on topography is not always clear. A potential explanation for this could be that the local modulation of the meteorological parameters that determine the FLS life cycle (e.g., relative humidity, wind) scales with the topographic features. In areas with moderate topography, the topography-induced local modulation of the meteorological setting would then have a weaker effect on the resulting geographic patterns of formation and dissipation times than in mountainous areas. In general, topographic features are only modulating the meteorological drivers responsible for FLS formation and dissipation. As has been shown in previous studies (Pauli *et al.*, 2020) meteorological factors are the main drivers of FLS occurrence over central Europe. In addition, the presented formation and dissipation times should be

interpreted with care over areas with a low sample size or high topographic variability, as the pixel size of the product (3–5 km, depending on the exact position) is too large to be able to depict small-scale variations in FLS.

Besides topography, the proximity to the sea is also important for the timing of FLS formation and dissipation. In general, coastal fog is strongly influenced by the meteorological conditions and ocean–atmosphere interactions (Gultepe *et al.*, 2021). The results presented here show a clear pattern of FLS formation at sunrise at the coast of the Mediterranean Sea in summer (Figure 9). According to Azorin-Molina *et al.* (2009) humid winds from the Mediterranean Sea in combination with mountain ranges close to the coastline can lead to FLS occurrence at the Mediterranean coast. Therefore, the diurnal cycle of the coastal circulation is likely a main driver of the observed patterns in FLS formation and dissipation times at the Mediterranean coast. At the Atlantic coast of northern Spain, blocking of FLS by the Cantabrian mountains (Egli

et al., 2017) and upwelling (Alvarez *et al.*, 2010) might be important for FLS formation, as the latter plays an important role in other FLS-prone regions such as at the southwestern African coast (Olivier and Stockton, 1989; Cermak, 2012; Andersen *et al.*, 2020). Close to the French Atlantic coast over the Landes forest south of 45°N, FLS forms earlier over the forest (around midnight) than over its surroundings (FLS formation in the morning), particularly in spring and summer. This is in line with enhanced nighttime FLS occurrence over this forest compared to its surroundings shown in Pauli *et al.* (2022), potentially due to enhanced emissions of biogenic volatile organic compounds over the forest, which can serve as cloud condensation nuclei (Spracklen *et al.*, 2008; Kammer *et al.*, 2018).

Another driving factor for the observed patterns is the solar radiation. As stated above, this is especially true for the dissipation time, where processes related to downwelling solar radiation (absorption inside the FLS layer, sensible heat flux) more strongly influence the dissipation of FLS compared to other, more subtle, drivers (Wærsted *et al.*, 2019). Formation can occur through various pathways during the day or during the night with formation patterns showing a much higher variability. To focus on specific FLS events and to unravel different formation and dissipation pathways, one could filter for stationary FLS events using image detection techniques or filter for meteorological conditions.

The higher number of formation and dissipation events over cities does not transfer to a difference of formation and dissipation time between cities and the surrounding land. In contrast to the literature (cf. Yan *et al.* (2020)) earlier dissipation over cities is not visible in the shown climatological means. On the one hand, this may be due to the assignment of the dissipation and formation times in % to different daytime and nighttime classes (Table 1) and the subsequent calculation of the mode, which could be investigated in more detail by looking at the raw formation and dissipation times over cities and surrounding areas. On the other hand, as discussed above, the FLS data set is likely to be flawed over cities during daytime, and thus misclassifications are likely to superimpose the actual patterns in the first place. Applying the proposed logistic regression algorithm to a robust high-resolution cloud mask over cities (Fuchs *et al.*, 2022) could add to our knowledge on the FLS life cycle over urban areas.

As these discussions on the possible processes underlying the geographic formation and dissipation patterns remain speculative, explicit regional analyses on the drivers of FLS formation and dissipation time are necessary. In addition, the potential influence of multilayer cloud situations and misclassifications on the presented FLS formation and dissipation time have to be considered

for the interpretation of the results. In a regional study, the FLS data set by Egli *et al.* (2017) used as a basis for this study has been shown to agree well with active sensor data (Pauli *et al.*, 2022). The formation and dissipation time patterns shown with this novel FLS formation and dissipation data set are also in line with LES and modelling studies over Europe (cf. Roach, 1995; Haeffelin *et al.*, 2010; Bergot, 2016; Steeneveld and de Bode, 2018), showing FLS formation in the night and dissipation after sunrise. While modelling, LES studies and local measurements display the FLS life cycle with high temporal resolution at a specific site and can also include the vertical component of an FLS event, the data set presented here provides a geographic perspective on formation and dissipation time over the whole of Central Europe.

5 | CONCLUSIONS

The central aim of this study was to investigate spatial patterns of FLS formation and dissipation times over Central Europe. For this purpose, an algorithm was designed which applies logistic regression to a binary satellite-based FLS cloud mask. With the novel data set, FLS formation and dissipation times were investigated, largely confirming known patterns of formation during the night and dissipation in the morning or in the afternoon. In general, FLS occurrence, formation and dissipation are dependent on various drivers (cf. Roach, 1995; Gultepe *et al.*, 2007a; Price, 2019; Pauli *et al.*, 2020). The results presented here underline the importance of topography-induced modulation of meteorology for FLS formation and dissipation. In mountain ranges, FLS forms most frequently at sunset and dissipates in the morning. At lower altitudes, such as in large-scale river valleys, FLS most commonly forms around sunrise and dissipates in the afternoon. Furthermore, we find a higher variability in formation times than in dissipation times, with the latter being much more dependent on solar radiation. The data set adds a geographic component to our knowledge of FLS formation and dissipation and provides a basis for future studies.

In the future, a preprocessing step could be implemented by adding a filter to study more specifically stationary FLS situations which may be indicative of radiation fog, for example using image detection techniques or focusing on specific meteorological conditions. The new algorithm can also be applied to other existing satellite-based FLS data sets with a high temporal resolution over regions where FLS are an important component of the climate and environment and station measurements are lacking, such as in the Namib Desert (Andersen and Cermak, 2018), and can be compared to diurnal patterns identified there so far (Andersen *et al.*, 2019). Furthermore

this data set holds promise to help better understand the drivers of FLS formation and dissipation at continental scales.

ACKNOWLEDGEMENTS

We thank two anonymous reviewers and Stephanie West-erhuis for their careful reviews which have helped improve the manuscript. E.P. has been financially supported by the Graduate Funding of the German States Program.

CONFLICT OF INTEREST

The authors declare that they have no known competing financial interests or personal relationships that could have appeared to influence the work reported in this paper.

AUTHOR CONTRIBUTIONS

Eva Pauli: Conceptualization, formal analysis, investigation, methodology, visualization, writing (original draft), writing (review and editing). **Jan Cermak:** Conceptualization, methodology, writing (review and editing). **Hendrik Andersen:** Methodology, writing (review and editing).

DATA AVAILABILITY STATEMENT

The fog and low stratus cloud data set serving as a basis for the algorithm can be downloaded from http://vhrz669.hrz.uni-marburg.de/lcrs/data_pre.do?citid=291. The formation and dissipation time data set is available at <https://doi.org/10.5445/IR/1000141293> (both accessed 25 March 2022).

ORCID

Eva Pauli  <https://orcid.org/0000-0002-5506-4736>

Jan Cermak  <https://orcid.org/0000-0002-4240-595X>

Hendrik Andersen  <https://orcid.org/0000-0003-2983-8838>

REFERENCES

- Alvarez, I., Gomez-Gesteira, M., deCastro, M., Gomez-Gesteira, J. and Dias, J. (2010) Summer upwelling frequency along the western Cantabrian coast from 1967 to 2007. *Journal of Marine Systems*, 79(1), 218–226. <https://doi.org/10.1016/j.jmarsys.2009.09.004>.
- American Meteorological Society (2012). Fog, in Glossary of Meteorology. Boston, MA: American Meteorological Society. <http://glossary.ametsoc.org/wiki/fog>.
- Andersen, H. and Cermak, J. (2018) First fully diurnal fog and low cloud satellite detection reveals life cycle in the Namib. *Atmospheric Measurement Techniques*, 11(10), 5461–5470. <https://doi.org/10.5194/amt-11-5461-2018>.
- Andersen, H., Cermak, J., Solodovnik, I., Lelli, L. and Vogt, R. (2019) Spatiotemporal dynamics of fog and low clouds in the Namib unveiled with ground- and space-based observations. *Atmospheric Chemistry and Physics*, 19(7), 4383–4392. <https://doi.org/10.5194/acp-19-4383-2019>.
- Andersen, H., Cermak, J., Fuchs, J., Knippertz, P., Gaetani, M., Quinting, J., Sippel, S. and Vogt, R. (2020) Synoptic-scale controls of fog and low-cloud variability in the Namib Desert. *Atmospheric Chemistry and Physics*, 20(6), 3415–3438. <https://doi.org/10.5194/acp-20-3415-2020>.
- Appelquist, S., Gahrs, G.E., Pfeffer, R.L. and Niu, X.-F. (2002) Comparison of methodologies for probabilistic quantitative precipitation forecasting. *Weather and Forecasting*, 17(4), 783–799. [https://doi.org/10.1175/1520-0434\(2002\)017<0783:COMFPQ>2.0.CO;2](https://doi.org/10.1175/1520-0434(2002)017<0783:COMFPQ>2.0.CO;2).
- Azarin-Molina, C., Sanchez-Lorenzo, A. and Calbo, J. (2009) A climatological study of sea breeze clouds in the southeast of the Iberian Peninsula (Alicante, Spain). *Atmosfera*, 22(1), 33–49.
- Bendix, J. (1994) Fog climatology of the Po Valley. *Rivista di meteorologia aeronautica*, 54(3-4), 25–36.
- Bendix, J. (2002) A satellite-based climatology of fog and low-level stratus in Germany and adjacent areas. *Atmospheric Research*, 64(1), 3–18. [https://doi.org/10.1016/S0169-8095\(02\)00075-3](https://doi.org/10.1016/S0169-8095(02)00075-3).
- Bendix, J., Thies, B., Nauss, T. and Cermak, J. (2006) A feasibility study of daytime fog and low stratus detection with TERRA/AQUA-MODIS over land. *Meteorological Applications*, 13(2), 111–125. <https://doi.org/10.1017/S1350482706002180>.
- Bergot, T. (2016) Large-eddy simulation study of the dissipation of radiation fog. *Quarterly Journal of the Royal Meteorological Society*, 142, 1029–1040. <https://doi.org/10.1002/qj.2706>
- Bisong, E. (2019). Logistic Regression, pp 243–250 in Building Machine Learning and Deep Learning Models on Google Cloud Platform. Berkeley, CA: Apress, DOI 10.1007/978-1-4842-4470-8_20, (to appear in print).
- Bruijnzeel, L.A., Eugster, W. and Burkard, R. (2006). Fog as a hydrologic input, in Encyclopedia of Hydrological Sciences, Anderson, M., McDonnell, J. (eds), DOI 10.1002/0470848944.hsa041, (to appear in print).
- Cermak, J. (2006). SOFOS – A new satellite-based operational fog observation scheme. PhD thesis, Philipps-Universität Marburg, Germany.
- Cermak, J. (2012) Low clouds and fog along the southwestern African coast – Satellite-based retrieval and spatial patterns. *Atmospheric Research*, 116, 15–21. <https://doi.org/10.1016/j.atmosres.2011.02.012>.
- Cermak, J. (2018) Fog and low cloud frequency and properties from active-sensor satellite data. *Remote Sensing*, 10(8), 1209. <https://doi.org/10.3390/rs10081209>.
- Cermak, J. and Bendix, J. (2007) Dynamical nighttime fog/low stratus detection based on Meteosat SEVIRI data: a feasibility study. *Pure and Applied Geophysics*, 164(6-7), 1179–1192. <https://doi.org/10.1007/s00024-007-0213-8>.
- Cermak, J. and Bendix, J. (2008) A novel approach to fog/low stratus detection using Meteosat 8 data. *Atmospheric Research*, 87(3), 279–292. <https://doi.org/10.1016/j.atmosres.2007.11.009>.
- Cermak, J. and Bendix, J. (2011) Detecting ground fog from space – a microphysics-based approach. *International Journal of Remote Sensing*, 32(12), 3345–3371. <https://doi.org/10.1080/01431161003747505>.
- Cermak, J., Eastman, R.M., Bendix, J. and Warren, S.G. (2009) European climatology of fog and low stratus based on geostationary satellite observations. *Quarterly Journal of the Royal*

- Meteorological Society*, 135, 2125–2130. <https://doi.org/10.1002/qj.503>.
- Dupont, J.-C., Haeffelin, M., Protat, A., Bouniol, D., Boyouk, N. and Morille, Y. (2012) Stratus-fog formation and dissipation: a 6-day case study. *Boundary-Layer Meteorology*, 143(1), 207–225. <https://doi.org/10.1007/s10546-012-9699-4>.
- Duynkerke, P.G. (1991) Radiation fog: a comparison of model simulation with detailed observations. *Monthly Weather Review*, 119(2), 324–341. [https://doi.org/10.1175/1520-0493\(1991\)119<0324:RFACOM>2.0.CO;2](https://doi.org/10.1175/1520-0493(1991)119<0324:RFACOM>2.0.CO;2).
- Egli, S., Thies, B., Drönner, J., Cermak, J. and Bendix, J. (2017) A 10-year fog and low stratus climatology for Europe based on Meteosat Second Generation data. *Quarterly Journal of the Royal Meteorological Society*, 143, 530–541. <https://doi.org/10.1002/qj.2941>.
- Ellrod, G.P. and Gultepe, I. (2007). Inferring low cloud-base heights at night for aviation using satellite infrared and surface temperature data, pp. 1193–1205 in *Fog and Boundary Layer Clouds: Fog Visibility and Forecasting*, Gultepe, I. (ed.) Basel, Switzerland: Birkhäuser.
- EUMETSAT (2019). Algorithm Theoretical Basis Document (ATBD) Meteosat Solar Surface Radiation and effective Cloud Albedo Climate Data Records – Heliosat (SARAH-2), Darmstadt, Germany. Technical Report.
- Fuchs, J., Andersen, H., Cermak, J., Pauli, E. and Roebeling, R. (2022) High-resolution satellite-based cloud detection for the analysis of land surface effects on boundary-layer clouds. *Atmospheric Measurement Techniques Discussions*, 2022, 1–22. <https://doi.org/10.5194/amt-2022-36>.
- Fuzzi, S., Facchini, M.C., Orsi, G., Lind, J.A., Wobrock, W., Kessel, M., Maser, R., Jaeschke, W., Enderle, K.H., Arends, B.G., Berner, A., Solly, I., Kruijs, C., Reischl, G., Pahl, S., Kaminski, U., Winkler, P., Ogren, J.A., Noone, K.J., Hallberg, A., Fierlinger-Oberlininger, H., Puxbaum, H., Marzorati, A., Hansson, H.-C., Wiedensohler, A., Svenningsson, I.B., Martinsson, B.G., Schell, D. and Georgii, H.W. (1992) The Po Valley fog experiment 1989. *Tellus B*, 44(5), 448–468. <https://doi.org/10.1034/j.1600-0889.1992.t01-4-00002.x>.
- Gottlieb, T.R., Eckardt, F.D., Venter, Z.S. and Cramer, M.D. (2019) The contribution of fog to water and nutrient supply to *Arthroa leubnitziae* in the central Namib Desert, Namibia. *Journal of Arid Environments*, 161, 35–46. <https://doi.org/10.1016/j.jaridenv.2018.11.002>.
- Gultepe, I., Tardif, R., Michaelides, S., Cermak, J., Bott, A., Bendix, J., Müller, M.D., Pagowski, M., Hansen, B., Ellrod, G., Jacobs, W., Toth, G. and Cober, S.G. (2007a) Fog research: a review of past achievements and future perspectives. *Pure and Applied Geophysics*, 164, 1121–1159. <https://doi.org/10.1007/s00024-007-0211-x>.
- Gultepe, I., Pagowski, M. and Reid, J. (2007b) A satellite-based fog detection scheme using screen air temperature. *Weather and Forecasting*, 22(3), 444–456. <https://doi.org/10.1175/WAF1011.1>.
- Gultepe, I., Heymsfield, A.J., Fernando, H.J.S., Paradyak, E., Dorman, C.E., Wang, Q., Creegan, E., Hoch, S.W., Flagg, D.D., Yamaguchi, R., Krishnamurthy, R., Gaberšek, S., Perrie, W., Perelet, A., Singh, D.K., Chang, R., Nagare, B., Wagh, S. and Wang, S. (2021) A review of coastal fog microphysics during C-FOG. *Boundary-Layer Meteorology*, 181(2), 227–265. <https://doi.org/10.1007/s10546-021-00659-5>.
- Haeffelin, M., Bergot, T., Elias, T., Tardif, R., Carrer, D., Chazette, P., Colomb, M., Drobinski, P., Dupont, E., Dupont, J.-C., Gomes, L., Musson-Genon, L., Pietras, C., Plana-Fattori, A., Protat, A., Rangognio, J., Raut, J.-C., Rmy, S., Richard, D., Sciare, J. and Zhang, X. (2010) Parisfog: shedding new light on fog physical processes. *Bulletin of the American Meteorological Society*, 91(6), 767–783. <https://doi.org/10.1175/2009BAMS2671.1>.
- Herman, G.R. and Schumacher, R.S. (2018) Dendrology in numerical weather prediction: what random forests and logistic regression tell us about forecasting extreme precipitation. *Monthly Weather Review*, 146(6), 1785–1812. <https://doi.org/10.1175/MWR-D-17-0307.1>.
- Kalthoff, N., Binder, H.-J., Kossmann, M., Vögtlin, R., Corsmeier, U., Fiedler, F. and Schlager, H. (1998) Temporal evolution and spatial variation of the boundary layer over complex terrain. *Atmospheric Environment*, 32(7), 1179–1194. [https://doi.org/10.1016/S1352-2310\(97\)00193-3](https://doi.org/10.1016/S1352-2310(97)00193-3).
- Kammer, J., Perraudin, E., Flaud, P.-M., Lamaud, E., Bonnefond, J. and Villenave, E. (2018) Observation of nighttime new particle formation over the French Landes forest. *Science of The Total Environment*, 621, 1084–1092. <https://doi.org/10.1016/j.scitotenv.2017.10.118>.
- Karimi, M. (2020) Direct numerical simulation of fog: the sensitivity of a dissipation phase to environmental conditions. *Atmosphere*, 11(1), 12. <https://doi.org/10.3390/atmos11010012>.
- Köhler, C., Steiner, A., Saint-Drenan, Y.-M., Ernst, D., Bergmann-Dick, A., Zirkelbach, M., Bouallègue, Z.B., Metzinger, I. and Ritter, B. (2017) Critical weather situations for renewable energies – Part B: low stratus risk for solar power. *Renewable Energy*, 101, 794–803. <https://doi.org/10.1016/j.renene.2016.09.002>.
- Kneringer, P., Dietz, S.J., Mayr, G.J. and Zeileis, A. (2019) Probabilistic nowcasting of low-visibility procedure states at Vienna International Airport during the cold season. *Pure and Applied Geophysics*, 176(5), 2165–2177. <https://doi.org/10.1007/s00024-018-1863-4>.
- Leigh, R.J., Drake, L. and Thampapillai, D.J. (1998) An economic analysis of terminal aerodrome forecasts with special reference to Sydney Airport. *Journal of Transport Economics and Policy*, 32(3), 377–392.
- Lever, J., Krzywinski, M. and Altman, N. (2016) Logistic regression. *Nature Methods*, 13, 541–542. <https://doi.org/10.1038/nmeth.3904>.
- López, L. and Sánchez, J. (2009) Discriminant methods for radar detection of hail. *Atmospheric Research*, 93(1), 358–368. <https://doi.org/10.1016/j.atmosres.2008.09.028>.
- Maalick, Z., Kühn, T., Korhonen, H., Kokkola, H., Laaksonen, A. and Romakkaniemi, S. (2016) Effect of aerosol concentration and absorbing aerosol on the radiation fog life cycle. *Atmospheric Environment*, 133, 26–33. <https://doi.org/10.1016/j.atmosenv.2016.03.018>.
- Olivier, J. and Stockton, P.L. (1989) The influence of upwelling extent upon fog incidence at Lüderitz, southern Africa. *International Journal of Climatology*, 9(1), 69–75. <https://doi.org/10.1002/joc.3370090106>.
- Pagowski, M., Gultepe, I. and King, P. (2004) Analysis and modeling of an extremely dense fog event in southern Ontario. *Journal of Applied Meteorology*, 43(1), 3–16. [https://doi.org/10.1175/1520-0450\(2004\)043<0003:AAMOAE>2.0.CO;2](https://doi.org/10.1175/1520-0450(2004)043<0003:AAMOAE>2.0.CO;2).

- Pauli, E., Andersen, H., Bendix, J., Cermak, J. and Egli, S. (2020) Determinants of fog and low stratus occurrence in continental central Europe – a quantitative satellite-based evaluation. *Journal of Hydrology*, 591. <https://doi.org/10.1016/j.jhydrol.2020.125451>.
- Pauli, E., Cermak, J. and Teuling, A.J. (2022) Enhanced nighttime fog and low stratus occurrence over the Landes forest, France. *Geophysical Research Letters*, 49(5). <https://doi.org/10.1029/2021GL097058>.
- Price, J. (2019) On the formation and development of radiation fog: an observational study. *Boundary-Layer Meteorology*, 172(2), 167–197. <https://doi.org/10.1007/s10546-019-00444-5>.
- Roach, W.T. (1995) Back to basics: Fog: Part 2 – the formation and dissipation of land fog. *Weather*, 50(1), 7–11.
- Scherrer, S.C. and Appenzeller, C. (2014) Fog and low stratus over the Swiss Plateau – a climatological study. *International Journal of Climatology*, 34(3), 678–686. <https://doi.org/10.1002/joc.3714>.
- Spracklen, D.V., Bonn, B. and Carslaw, K.S. (2008) Boreal forests, aerosols and the impacts on clouds and climate. *Philosophical Transactions of the Royal Society A*, 366(1885), 4613–4626. <https://doi.org/10.1098/rsta.2008.0201>.
- Steenefeld, G.-J. and de Bode, M. (2018) Unravelling the relative roles of physical processes in modelling the life cycle of a warm radiation fog. *Quarterly Journal of the Royal Meteorological Society*, 144, 1539–1554. <https://doi.org/10.1002/qj.3300>.
- Torregrosa, A., Combs, C. and Peters, J. (2016) GOES-derived fog and low cloud indices for coastal north and central California ecological analyses. *Earth and Space Science*, 3(2), 46–67. <https://doi.org/10.1002/2015EA000119>.
- Vautard, R., Yiou, P. and Van Oldenborgh, G.J. (2009) Decline of fog, mist and haze in Europe over the past 30 years. *Nature Geoscience*, 2(2), 115–119. <https://doi.org/10.1038/ngeo414>.
- Wærsted, E.G., Haeffelin, M., Steeneveld, G.-J. and Dupont J.-C. (2019) Understanding the dissipation of continental fog by analysing the LWP budget using idealized LES and *in situ* observations. *Quarterly Journal of the Royal Meteorological Society*, 145, 784–804. <https://doi.org/10.1002/qj.3465>.
- Wu, W. and Zhang, L. (2013) Comparison of spatial and non-spatial logistic regression models for modeling the occurrence of cloud cover in northeastern Puerto Rico. *Applied Geography*, 37, 52–62. <https://doi.org/10.1016/j.apgeog.2012.10.012>.
- Yan, S., Zhu, B., Huang, Y., Zhu, J., Kang, H., Lu, C. and Zhu, T. (2020) To what extents do urbanization and air pollution affect fog?. *Atmospheric Chemistry and Physics*, 20(9), 5559–5572. <https://doi.org/10.5194/acp-20-5559-2020>.

SUPPORTING INFORMATION

Additional supporting information may be found online in the Supporting Information section at the end of this article.

How to cite this article: Pauli, E., Cermak, J. & Andersen, H. (2022) A satellite-based climatology of fog and low stratus formation and dissipation times in central Europe. *Quarterly Journal of the Royal Meteorological Society*, 148(744), 1439–1454. Available from: <https://doi.org/10.1002/qj.4272>